Proceedings of the 17th World Congress
The International Federation of Automatic Control
Seoul, Korea, July 6-11, 2008

Linear Robust Control for a Nonlinear Active Suspension Model Considering Variable Payload

Michael Herrnberger*, Dominik Mäder*, Boris Lohmann*

** Institute of Automatic Control, Technische Universität München, Munich, Germany (e-mail: herrnberger@tum.de, dmaeder@mytum.de, lohmann@tum.de)*

Abstract: The control of active suspension systems is described in many publications over the last decades. However, often only idealized linear models are used for control design and simulations, what can lead to wrong conclusions regarding controller performance and energy costs. Therefore, this paper presents a nonlinear passive suspension model of a quarter car test-rig currently built up at the Institute of Automatic Control which can be extended with models of active elements. Furthermore it is lined out, how a robust controller can be synthesized for this system. For this purpose the nonlinear model is linearized around the equilibrium point and parametric model uncertainties are introduced together with performance weighting functions. In order to include the influence of the variable chassis payload into the design process, a trim point uncertainty is added which completes the structured uncertainty model. With this a modern robust control design approach using the structured singular value can be presented, considering different chassis masses and their influence on the linearization point. Finally it is demonstrated, how robust performance or robust stability can be analyzed if a linear controller already exists.

1. INTRODUCTION

Active suspension systems play a more and more important role in the automotive industry because they can ease the conflict between passenger comfort and ride safety what can be done by passive systems only in a very limited way. Therefore a quarter car test-rig of a quadricycle is currently built up at the Institute of Automatic Control which offers the possibility to analyze different semi-active and active suspension configurations and control approaches.

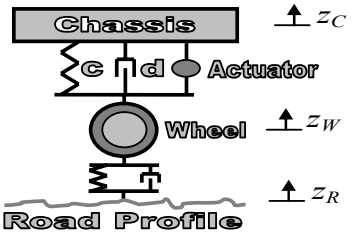

Fig. 1. Linear active suspension model

There exist several ways of modeling the system, the most simple of which is a linear quarter car model as it is shown in Fig. 1 and presented in innumerable books and papers, e.g. (Mitschke *et al*., 2004). However, here a model should be developed which reflects the system behavior in a quite exact way in order to allow for a control design which can be directly applied to the real test-rig. For this purpose either a black box model can be experimentally identified or a physical nonlinear model must be derived.

For this study a physical nonlinear model of the suspension is chosen because it offers the advantage that not only arbitrary control laws but also changes in the test-rig configuration can be quite realistically examined in simulations before applying them to the real system. However, even a nonlinear model is still only an approximation of the real system using several simplifications and idealizations in order to limit model complexity. Furthermore some parts of the model, like spring, damper or friction characteristics, can only be gained by identification. Nevertheless, once the model is built up and validated, it represents an excellent simulation tool.

As beneficial as a nonlinear model may be for simulation purposes, as problematic can it be for controller design or analysis because many classical design approaches demand a linear model. That is why in this paper also the linearization of the nonlinear model around the equilibrium point will be presented. For linear models there exist plenty of active suspension control methods. In (Venhovens, 1993) a good overview over different designs and configurations can be found. There also exist several robust control approaches using either H_∞ (e.g. Fialho *et al*., 2000) or μ methods (e.g. Lauwerys *et al*., 2004). Those approaches focus on the linear, with parametric or dynamic uncertainties augmented system in Fig. 1. In comparison to that, in this paper robust control methods are outlined which deal with an uncertain linear model that is derived from the nonlinear one. Hence, it depends on the equilibrium point which again is a function of the variable payload. The robustness analysis or controller synthesis is accomplished with the structured singular value using a structured uncertainty model which contains different types of uncertainties.

In order to come up for neglected higher order dynamics, nonlinearities and other modeling errors, a multiplicative system input uncertainty is added to the model. The nominal

spring and damper constants are augmented with own parametric uncertainties, because they can show high nonlinear behavior (bendings in the spring characteristic, damping constant dependent on direction and manual pre-configuration).

Now the fact that the equilibrium point and the system dynamics are a function of the chassis payload, e.g. the driver mass, must be considered. If no gain-scheduling is applied on the controller, the robustness with respect to those payload variations must be challenged. Therefore the dependency of the model on the chassis mass is included into the model using a trim point uncertainty. By that a very modern and effective way of synthesizing or analyzing robust controllers for active suspensions is demonstrated. Another application of this trim point uncertainty concept can be found in (Herrnberger *et al*., 2007) where it is used for the robustness analysis of a flight control system.

2. NONLINEAR SUSPENSION MODEL

The nonlinear suspension model is based on the nonlinear quarter car structure depicted in Fig. 2. Although it is nonlinear, still some assumptions are made, e.g. that the masses are lumped in two chassis and wheel point masses and that there is only one friction force acting parallel to the spring, damper and actuator forces.

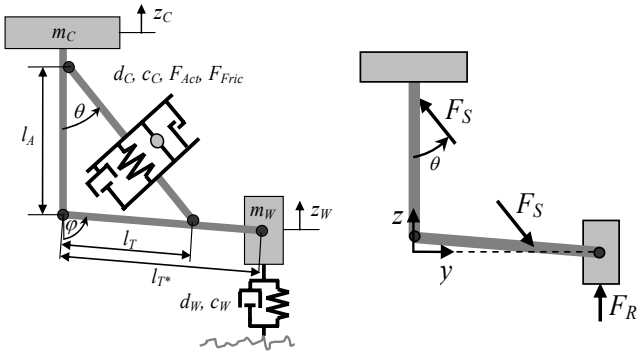

Fig. 2. Nonlinear active suspension model and forces

2.1 EQUATIONS OF MOTION

The differential equations of motion can be derived with Lagrange mechanics (Goldstein *et al*., 2002). Details on the calculations can be found in (Mäder, 2007). A logical choice for the generalized coordinates is

$$\boldsymbol{q} = [z_C \;\; \varphi]^{\mathrm{T}}. \tag{1}$$

The kinetic energy T of the system contains the kinetic energy of the two point masses.

$$T_C = \frac{m_C}{2}\dot{z}_C^2 \qquad T_W = \frac{m_W}{2}\left(\dot{\varphi}^2 \cdot l_{T*}^2 + 2 \cdot \sin(\varphi) \cdot \dot{\varphi} \cdot l_{T*} \cdot \dot{z}_C + \dot{z}_C^2\right) \tag{2}$$

The term for the potential energy is set to 0 here because the first source of potential energy, the gravity, is not part of the model due to the fact that only motions around the equilibrium point are treated; the second source, the spring force, is classified as nonconservative in order to allow for a nonlinear spring characteristic. Beside the spring forces, the nonconservative forces also contain the damper, friction and actuator forces. They are summed up as "suspension force" F_S and "road force" F_R (see Fig. 2).

In the *y*-*z*-frame the nonconservative force vectors can be represented as

$$\boldsymbol{F_{S1}} = \begin{bmatrix} -F_S \cdot \sin(\theta) \\ F_S \cdot \cos(\theta) \end{bmatrix}, \quad \boldsymbol{F_{S2}} = \begin{bmatrix} F_S \cdot \sin(\theta) \\ -F_S \cdot \cos(\theta) \end{bmatrix}, \quad \boldsymbol{F_R} = \begin{bmatrix} 0 \\ F_R \end{bmatrix} \tag{3}$$

what leads to the generalized nonconservative force vector

$$\boldsymbol{Q_{nc}} = \sum_{i=\{S1,S2,R\}} \left[\frac{\partial \boldsymbol{r}_i}{\partial \boldsymbol{q}_i}\right]^{\mathrm{T}} \boldsymbol{F}_i = \begin{bmatrix} F_R \\ \sin(\varphi)\left(\dfrac{-l_A l_T F_S}{l_S} + l_{T*} F_R\right) \end{bmatrix} \tag{4}$$

with $l_S = l_S(\varphi) = \sqrt{l_A^2 + l_T^2 + 2 l_A l_T \cos(\varphi)}$ where $\boldsymbol{r}_i$ represents the positions of the force application points. According to Lagrange's equation

$$\left(\frac{d}{dt}\left(\frac{\partial T}{\partial \dot{\boldsymbol{q}}}\right)\right)^{\mathrm{T}} - \left(\frac{\partial T}{\partial \boldsymbol{q}}\right)^{\mathrm{T}} + \left(\frac{\partial V}{\partial \boldsymbol{q}}\right)^{\mathrm{T}} = \boldsymbol{Q}_{nc} \tag{5}$$

the equations of motion of the suspension system can be derived with $m_S = m_S(\varphi) = \left(m_C + \cos^2(\varphi) \cdot m_W\right)$ as

$$\begin{aligned} \ddot{\varphi} &= \frac{m_C \sin(\varphi) F_R}{m_W l_{T*} m_S} - \frac{l_C l_T (m_C + m_W)\sin(\varphi) F_S}{m_W l_{T*}^2 m_S l_S} + \frac{m_W \cdot \sin(\varphi) \cdot \cos(\varphi) \cdot \dot{\varphi}^2}{m_S}, \\ \ddot{z}_C &= \frac{\cos^2(\varphi) F_W}{m_S} + \frac{l_A l_T \sin^2(\varphi) F_S}{l_{T*} m_S l_S} - \frac{m_W \cdot l_{T*} \cdot \cos(\varphi_T) \cdot \dot{\varphi}^2}{m_S}. \end{aligned} \tag{6}$$

Finally the nonconservative forces are defined in (7). Here for the road force, linear spring and damper characteristics are assumed (which can be replaced by a better model later), while for the suspension force a nonlinear characteristic is considered. The latter can be identified in experiments.

$$\begin{aligned} F_R &= -c_W(z_W - z_R) - d_W(\dot{z}_W - \dot{z}_R) \\ &= -c_W(z_C - l_{T*}\cos(\varphi) + l_{T*}\cos(\varphi_0) - z_R) \\ &\quad - d_W(\dot{z}_C + l_{T*}\sin(\varphi)\dot{\varphi} - \dot{z}_R) \end{aligned} \tag{7}$$

$$F_S = F_c(l_S - l_{S0}) + F_d(\dot{l}_S) + F_{Fric}(\dot{l}_S, t) + F_{Act}(t)$$

As it can be seen in (7), the nonconservative forces depend on the equilibrium point which is marked with the index 0. The equilibrium point itself is a function of the chassis mass which changes with the payload.

2.2 FRICTION MODEL

The friction force F_{Fric} in (7) is calculated with a friction model proposed in (Canudas de Wit *et al*., 1995) which uses Coulomb and Stribeck friction.

$$F_{Fric} = \begin{cases} -F_{ext}, & \text{if } |\dot{l}_S| \le \varepsilon \ \& \ |F_{ext}| \le F_{stat}(t), \\ -F_{stat}(t)\cdot \text{sign}(F_{ext}), & \text{if } |\dot{l}_S| \le \varepsilon \ \& \ |F_{ext}| > F_{stat}(t), \\ -F_{strib}^{del}\cdot \text{sign}(\dot{l}_S) - d_{visc} v_{rel}, & \text{if } |\dot{l}_S| > \varepsilon, \end{cases} \quad (8)$$
$$F_{strib}^{del} = \left(F_{coul} + (F_{stat}(t) - F_{coul})\cdot \exp(-|\dot{l}_S|/v_{strib})\right)/(T_{strib}s+1).$$

The details of the friction model in (8) should not be explained here as it represents not the main contribution of this paper. It should only be mentioned that it works with delayed static and Stribeck friction values in order to take lubrication film dynamics into account (e.g. hysteresis). Although the model is quite complicated it provides more realistic results than only using static and vicious friction. Not all parameters were exactly identified, yet, but Fig. 3 shows the friction force for a specific relative velocity profile with estimated parameters.

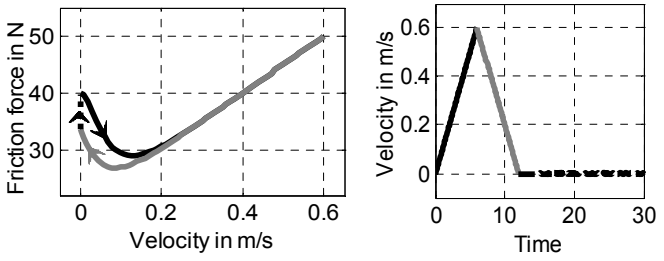

Fig. 3. Friction characteristic

3. LINEARIZATION OF THE STATE SPACE MODEL

As mentioned above, for the controller design / analysis presented in this paper a linear model is needed. Therefore the system from (6) is linearized in the equilibrium point of the suspension system which is defined by (9). Details and the full equations again can be found in (Mäder, 2007).

$$F_{S,0}(\varphi_0)\cdot(l_A + 2\cdot l_T\cdot\cos(\varphi_0))/l_{S,0}(\varphi_0) = m_C\cdot g \quad (9)$$

Measurements showed that $\varphi_0 = 75°$ for a chassis mass $m_C = 45\,\text{kg}$. If the nonlinear system is described by the nonlinear state space model

$$\dot{\boldsymbol{x}} = \boldsymbol{a}(\boldsymbol{x}) + \boldsymbol{b}(\boldsymbol{x})\boldsymbol{u} \quad \text{with}$$
$$\boldsymbol{x} = [z_C \ \dot{z}_C \ \varphi \ \dot{\varphi}]^{\mathrm{T}}, \quad \boldsymbol{u} = [z_R \ \dot{z}_R \ F_{Act}]^{\mathrm{T}},$$
$$\boldsymbol{a}(\boldsymbol{x}) = [x_2 \ a_2(\boldsymbol{x}) \ x_4 \ a_4(\boldsymbol{x})]^{\mathrm{T}},$$
$$\boldsymbol{b}(\boldsymbol{x}) = \boldsymbol{b}(\varphi) = \begin{pmatrix} 0 & 0 & 0 \\ \frac{\cos^2(\varphi)c_W}{m_S(x_3)} & \frac{\cos^2(\varphi)d_W}{m_S(x_3)} & \frac{l_A l_T \sin^2(\varphi)}{l_{T*} m_S I_S} \\ 0 & 0 & 0 \\ \frac{m_C\cdot\sin(\varphi)c_W}{l_{T*} d_W m_S(x_3)} & \frac{m_C\cdot\sin(\varphi)d_W}{l_{T*} d_W m_S(x_3)} & \frac{l_C l_T (m_C+m_W)\sin(\varphi)}{m_W l_{T*}^2 m_S I_S} \end{pmatrix}, \quad (10)$$

where $a_2(\boldsymbol{x})$ and $a_4(\boldsymbol{x})$ are defined by the equations in (6), then the in the equilibrium point linearized model can be written as

$$\dot{\boldsymbol{x}} = \boldsymbol{A}\boldsymbol{x} + \boldsymbol{B}\boldsymbol{u} \quad \text{with}$$
$$\boldsymbol{A} = \begin{bmatrix} 0 & 1 & 0 & 0 \\ a_{21} & a_{22} & a_{23} & a_{24} \\ 0 & 0 & 0 & 1 \\ a_{41} & a_{42} & a_{43} & a_{44} \end{bmatrix}, \quad \boldsymbol{B} = \boldsymbol{b}(\varphi_0). \quad (11)$$

The matrix elements of $\boldsymbol{A}$ are found to be

$$a_{21} = -\cos^2(\varphi_0)c_W/m_{S0}, \ a_{22} = a_{21}\cdot d_W/c_W,$$
$$a_{23} = K_1 c_{C0} + K_2, \ a_{24} = K_1 d_{C0} + K_3,$$
$$a_{41} = -m_C\sin(\varphi_0)c_W/(l_{T*}m_R m_{S0}), \ a_{42} = a_{41}\cdot d_W/c_W, \quad (12)$$
$$a_{43} = K_4 c_{C0} + K_5, \ a_{44} = K_4 d_{C0} + K_6,$$

where the $K_i = K_i(m_C, \varphi_0)$ are constants for a certain equilibrium point. The spring and damping constants c_{C0} and d_{C0}, which result from the suspension force in (7), need not consequently be the exact derivatives of the characteristics at the equilibrium point, but can also be user-defined mean values. The parameter d_{C0} also contains the viscous damping coefficient which results form the linearized friction force.

4. ACTUATORS AND SENSORS

For the active control of a suspension system an active element must be added, of course. For the test-rig a special linear motor will be used. While the exact nonlinear actuator modeling is often worth an own paper, here, for the first preliminary studies, the actuator will only be modeled as a simple linear second order system with time delay. By that, at least the most crucial actuator properties should be taken into account. The time delay τ, which is modeled as 1st order Padé approximation, represents the digital signal processing delays. Thus, the actuator is defined by

$$G_{Act} = \frac{(1-s\tau/2)}{(1+s\tau/2)}\cdot(T_{Act}^2 s^2 + 2d_{Act}T_{Act} + 1). \quad (13)$$

For the sensors equivalent second order systems with time delay are used. In the course of the test-rig project the actuator and sensor models will be improved.

5. UNCERTAINTY MODEL

For the design / analysis of a robust controller the linearized model of (11) is augmented with uncertainties and weighting functions. Most of the theory of uncertainty modeling and robust control design can be found in (Balas *et al.*, 1998), (Skogestad *et al.*, 1996) or (Zhou *et al.*, 1996). The basic procedure will only be briefly presented here because it is extensively investigated in many publications.

At first the system output must be chosen for feedback. Usually the chassis acceleration $\ddot{z}_C$ (or velocity $\dot{z}_C$ or position z_C) and the suspension deflection, which is here characterized by the angle φ, are used because they can rather easily be measured. By taking e.g. $\boldsymbol{y} = [\ddot{z}_C \ \varphi]^{\mathrm{T}}$ as output, the state space model of (11) can be completed:

$$\dot{\boldsymbol{x}} = \boldsymbol{A}\boldsymbol{x} + \boldsymbol{B}\boldsymbol{u}, \quad \boldsymbol{y} = \boldsymbol{C}\boldsymbol{x} + \boldsymbol{D}\boldsymbol{u} \quad \text{with}$$
$$\boldsymbol{C} = \begin{bmatrix} a_{21} & a_{22} & a_{23} & a_{24} \\ 0 & 0 & 1 & 0 \end{bmatrix}, \quad \boldsymbol{D} = \begin{bmatrix} b_{21} & b_{22} & b_{23} \\ 0 & 0 & 0 \end{bmatrix}. \tag{14}$$

5.1 MODEL UNCERTAINTIES

As it was mentioned in the introduction, due to nonlinear and by the driver switchable characteristics, the nominal suspension spring and damper constants are augmented with own parametric uncertainties,

$$c_{C0} = \bar{c}_{C0}\left(1+\eta_c\delta_c\right) \quad \text{and} \quad d_{C0} = \bar{d}_{C0}\left(1+\eta_d\delta_d\right), \tag{15}$$

where $\bar{c}_{C0}, \bar{d}_{C0}$ are the nominal mean values, η_c, η_d are the multiplicative uncertainty weights and δ_c, δ_d are the uncertainty variables, fulfilling $|\delta_i| \le 1$. The mean values $\bar{c}_{C0}, \bar{d}_{C0}$ and the uncertainty weights η_c, η_d can be modeled as functions of m_C, too. The weights must be chosen in such a way that they cover all values the parameters may assume in a sufficient large range around the equilibrium point.

To come up for the linearization errors in (11), the neglected higher order actuator dynamics in (13) and other possible parametric uncertainties (c_W etc.) a complex uncertainty is added in the actuator input channel. The augmented system can be transformed into a so called linear fractional representation (LFR) by adding new virtual inputs and outputs (Balas *et al*., 1998), as it is shown in Fig. 4.

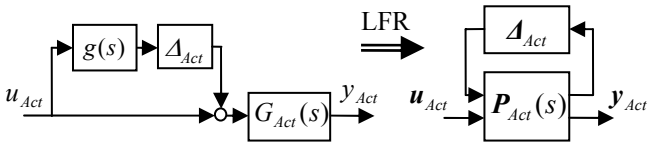

Fig. 4. Actuator input uncertainty and actuator LFR

$$\boldsymbol{P}_{Act}(s) = \begin{bmatrix} 0 & g(s) \\ G_{Act}(s) & G_{Act}(s) \end{bmatrix} \text{ with } \left\|\boldsymbol{\Delta}_{Act}\right\|_\infty \le 1 \tag{16}$$

5.2 TRIM POINT UNCERTAINTY

Until now the uncertainty modeling has only been done for one equilibrium point. Hence, in order to guarantee robustness for all possible chassis masses, either the controller synthesis / analysis must be done multiple times for a sufficient big set of possible masses or the chassis mass variation is included into the model with the help of a trim point uncertainty. Then with one single analysis / synthesis, the whole payload range can be taken into account.

As it was already outlined in (Herrnberger *et al*., 2007) for another application, the idea behind the "trim point uncertainty" is to approximate the dependency of the nominal system parameters on m_C by algebraic functions and to parameterize these functions with a variable δ_{TP} in such a way, that the whole range of trim values is covered when varying δ_{TP} from -1 to 1. Here the expression trim point is equal to the equilibrium point.

It should be mentioned that the uncertainty modeling can also be done in a more automated way with symbolic calculations which can also lead to uncertainty models of lower order, as it is proposed e.g. in (Hecker, 2007). However, in order to enhance the insight into the process and to make it more independent of special toolboxes, here the modeling is demonstrated in a more classical step-by-step way.

Combining (12) and (15) it can be seen that every single state space matrix element of $\boldsymbol{A}$, $\boldsymbol{B}$, $\boldsymbol{C}$, $\boldsymbol{D}$ can be represented by

$$a^{ik}(m_C, \varphi_0) = \alpha_A^{ik}(m_C, \varphi_0) + \beta_A^{ik}(m_C, \varphi_0) \cdot \delta_A^{ik}, \tag{17}$$

whereby $\alpha_A^{ik}, \beta_A^{ik}$ are trim point dependent constants and the δ_A^{ik} either represent δ_c or δ_d. As it is in (17), also in the following the modeling will only be presented for the $\boldsymbol{A}$-part, because the procedure is the same for $\boldsymbol{B}$, $\boldsymbol{C}$ and $\boldsymbol{D}$. If now, having according to (9) $\varphi_0 = \text{fct}(m_C)$ in mind, the trim range of m_C is mapped to a trim point uncertainty variable δ_{TP} like

$$m_C \in [m_{C\min}; m_{C\max}] \rightarrow \delta_{TP} \in [-1;1]\colon \ \delta_{TP}(m_C) = \frac{m_C - \overline{m}_C}{\frac{(m_{C\max} - m_{C\min})}{2}}, \tag{18}$$

then the values of the parameters $\alpha_A^{ik}, \beta_A^{ik}$ along the trim range can be approximated e.g. with rational functions which can be computed via least mean square regression for a set of trim points:

$$\frac{\lambda_{1A}^{ik} + \lambda_{2A}^{ik}\delta_{TP}}{1 + \lambda_{3A}^{ik}\delta_{TP}} \approx \alpha_A^{ik}(\delta_{TP}), \quad \frac{\nu_{1A}^{ik} + \nu_{2A}^{ik}\delta_{TP}}{1 + \nu_{3A}^{ik}\delta_{TP}} \approx \beta_A^{ik}(\delta_{TP}). \tag{19}$$

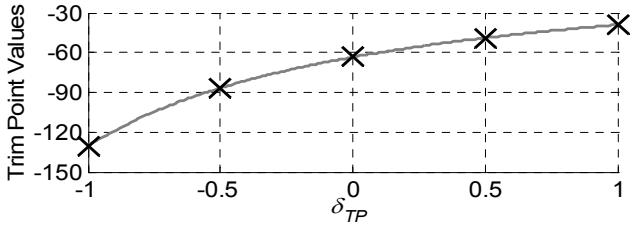

Fig. 5. Trim point approximation with rational functions

For this system rational functions allow for quite good approximations of $\alpha_A^{ik}, \beta_A^{ik}$ with neglectable errors, as it can exemplarily be seen in Fig. 5 for $\alpha_A^{21}(\delta_{TP})$ (x = five real values, solid line = approximation), and provide smaller uncertainty model dimensions than more complicated functions. Now, after substituting $\lambda_{4A}^{ik} = \lambda_{2A}^{ik} - \lambda_{1A}^{ik}\lambda_{3A}^{ik}$, in the state equations new virtual inputs $w_{1A}^{ik}, w_{2A}^{ik}, w_{3A}^{ik}$ and outputs $q_{1A}^{ik}, q_{2A}^{ik}, q_{3A}^{ik}$ can be added in order to separate the uncertainty variables in an own uncertainty matrix (as it was done in (16) and Fig. 4).

$$\begin{aligned} \dot{x}_A^i &= \sum_{k=1}^{4}\left(\lambda_{1A}^{ik}x^k + \nu_{1A}^{ik}w_{1A}^{ik} + \lambda_{4A}^{ik}w_{2A}^{ik} + \nu_{4A}^{ik}w_{3A}^{ik}\right), \\ q_{1A}^{ik} &= \frac{w_{1A}^{ik}}{\delta_A^{ik}} = x^k, \quad q_{2A}^{ik} = \frac{w_{2A}^{ik}}{\delta_{TP}} = x^k - \lambda_{3A}^{ik}w_{2A}^{ik}, \\ q_{3A}^{ik} &= \frac{w_{3A}^{ik}}{\delta_{TP}} = w_{1A}^{ik} - \nu_{3A}^{ik}w_{3A}^{ik} \end{aligned} \tag{20}$$

Finally a LFR of the suspension state space model can be created which contains the known constant values in $\boldsymbol{P}_S$ and all the δ_c, δ_d and δ_{TP} uncertainty variables in a sorted arrangement on the diagonal of $\boldsymbol{\Delta}_S$ (see Fig. 6). By merging the actuator LFR, the suspension system LFR and the sensor transfer functions, it is possible to represent the whole system together with a controller $\boldsymbol{R}$ in a closed loop LFR (Fig. 6). For more details (Herrnberger *et al*., 2007) can be consulted.

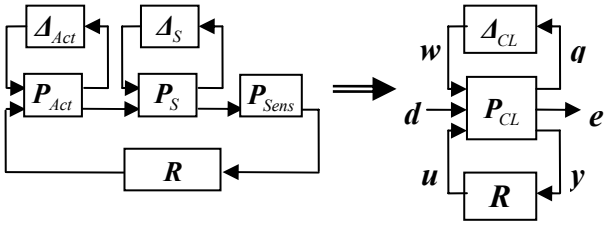

Fig. 6. Uncertain subsystems and closed loop LFR

6. CONTROLLER SYNTHESIS AND ANALYSIS

Basing on the closed loop LFR in Fig. 6 it is now quite easy to synthesize a robust controller or analyze an existing one via the μ methods. If a robust controller shall be designed, at first performance weighting functions must be added to the signals $\boldsymbol{d}$ and $\boldsymbol{e}$ in order to normalize the transfer functions according to the performance requirements. Here $\boldsymbol{d}$ denotes the disturbances which enter the system (road excitation and measurement noise), whereas $\boldsymbol{e}$ represents the error signals which should be minimized (e.g. the chassis acceleration or the dynamic wheel load). The frequency weighting functions are necessary because it is not possible to reduce all transfer functions from $\boldsymbol{d}$ to $\boldsymbol{e}$ in the same frequency range with the same magnitude. However, since it is not the focus of this paper to explain the definition of the weighting functions, it shall be referred to (Fialho *et al*., 2000) where a very good example for the design of the weights is given.

After adding the weights, which creates a new weighted error signal $\boldsymbol{e}^w$ and an extended system $\boldsymbol{P}_{CL}^w$, a complex unstructured "fake" uncertainty $\boldsymbol{\Delta}_F$ can be added to the system which connects the signals $\boldsymbol{d}$ and $\boldsymbol{e}^w$, see Fig. 7a. By that the robust performance problem can be treated as a robust stability problem (Balas *et al*., 1998). Then the design of the robust controller can be performed using the D-K-iteration, e.g. in Matlab, which is a numeric approximation of the μ synthesis and, due to the structured uncertainty matrix $\boldsymbol{\Delta}_{CL}^F = \mathrm{diag}(\boldsymbol{\Delta}_F, \boldsymbol{\Delta}_{CL})$, less conservative than the H_∞ design. It should be mentioned, that the trim point uncertainty can add some conservatism to the design when it is extrapolated to values $|\delta_{TP}| > 1$, as it may be the case during the synthesis process. Here a skew-μ approach could be helpful which limits δ_{TP} to the range between -1 and 1.

If already a controller exists, the robust performance of which should be proved, then standard numeric μ analysis can be applied on the block diagram shown in Fig. 7b. To generate the system $\boldsymbol{M}_{CL}$, the controller $\boldsymbol{R}$ is included into the system via a lower linear fractional transformation:

$$\boldsymbol{M}_{CL} = F_l(\boldsymbol{P}^w, \boldsymbol{R}) = \boldsymbol{P}_{12}^w \boldsymbol{R}(\boldsymbol{I} - \boldsymbol{P}_{22}^w \boldsymbol{R})^{-1} \boldsymbol{P}_{21}^w + \boldsymbol{P}_{11}^w . \tag{21}$$

If only the performance loop with $\boldsymbol{\Delta}_F$ is considered ($\boldsymbol{\Delta}_{CL}$ is empty) and, by definition, $\|\boldsymbol{\Delta}_F\|_\infty \le 1$, then the system is stable if $\|\boldsymbol{M}_{CL}\|_\infty < 1$ (Small Gain Theorem). That inequality is exactly what the H_∞ algorithm tries to prove. μ and H_∞ will yield identical results here. But if $\boldsymbol{\Delta}_{CL}$ is not empty, then, due to the structure of $\boldsymbol{\Delta}_{CL}^F$, $\mu(\boldsymbol{M}_{CL})$ will provide less conservative results than $\|\boldsymbol{M}_{CL}\|_\infty$ because its peak value along the frequency will be smaller than the H_∞ norm.

Mathematically μ is defined as the reciprocal value of the – in terms of the $\boldsymbol{H}_\infty$ norm – smallest perturbation $\boldsymbol{\Delta}_{CL}^F$ which drives the system to the border of instability. This happens when the determinant in (22) vanishes. Thus, the system is robust stable if (and only if) $\mu < 1$ for all frequencies.

$$\begin{aligned} \frac{1}{\mu(\boldsymbol{M}_{CL}(j\omega))} &= \inf_{\boldsymbol{\Delta}_{CL}} \left\{ \bar{\sigma}(\boldsymbol{\Delta}_{CL}^F) : \det\left(\boldsymbol{I} - \boldsymbol{\Delta}_{CL}^F \boldsymbol{M}_{CL}(j\omega)\right) = 0 \right\} \\ \mu(\boldsymbol{M}_{CL}(j\omega)) &= 0, \text{ if } \det\left(\boldsymbol{I} - \boldsymbol{\Delta}_{CL}^F \boldsymbol{M}_{CL}(j\omega)\right) \neq 0 \end{aligned} \tag{22}$$

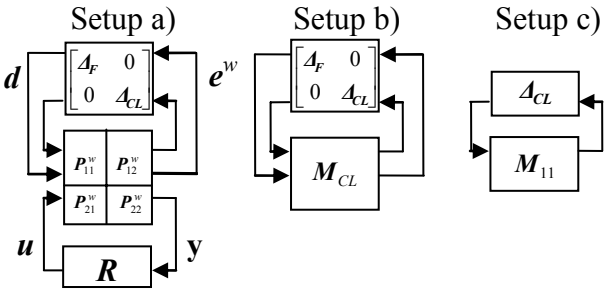

Fig. 7. LFR setup for a) μ synthesis, b) μ robust performance analysis, c) μ robust stability analysis

If only the robust stability of the controlled system must be examined, then only the part $\boldsymbol{M}_{11}$ of $\boldsymbol{M}_{CL}$, which is connected to $\boldsymbol{\Delta}_{CL}$, is used for μ analysis, see Fig. 7c.

7. ANALYSIS EXAMPLE

In order to illustrate the concept of trim point uncertainties a simple example for $\dot{z}_C$-feedback should be given. As described in (Mäder, 2007), the use of velocity feedback is not the best but a quite effective method compared with the simplicity of the approach. This example only focuses on the robust stability analysis in order to illustrate the effectiveness of the approach. For the first test a chassis mass variation from 45 kg to 125 kg was assumed (45 kg for no payload, 125 kg with driver / payload). The approximation with rational functions works excellent for this system, as shown in Fig. 5.

At first some nonlinear simulations were performed for different chassis masses and controller gains. Some of the parameters were estimated (e.g. for the friction model), because the model identification hasn't been completed, yet ($m_W = 19$, $c_W = 90000$, $d_W = 400$, $\bar{c}_C = 32200$, $\bar{d}_C = 1000$, $l_T = 0.14$, $l_{T*} = 0.3$, $l_A = 0.295$, $T_{Act} = 0.02$, $\tau_{Act} = 0.002$, $d_{Act} = 1$). For the street profile real measurement data was

used. The simulations showed that for $m_C = 45$ the system becomes unstable for controller gains $R \le -7000$, whereas for $m_C = 85$ an $R \ge -11000$ could be allowed. Furthermore in Fig. 8 the simulation results of the passive and the active configuration for $m_C = 45$ and $R = -3000$ were plotted. The active system yields a much better performance (the actuator forces were rather high, but not unrealistic).

For the stability analysis, first the parametric uncertainties were set to 0, using only a dynamic uncertainty $g(s) = (s+20)/(s+400)$ (i.e. 5% input uncertainty for low frequencies), in order to come up for linearization errors. Fig. 9 plots the μ upper and lower bounds for the same controllers that were examined in the simulations above: for $m_C \in [45;125]$, with $R = -5000$ the system is robust stable ($\mu < 1$) and for $R = -7000$ unstable ($\mu > 1$); for $m_C \in [80;125]$, with $R = -10000$ the system is still stable again. The results show, that simulation and analysis match very well which proves the presented methodology to be a promising approach.

In a final test the both parametric spring and damper uncertainties were set to 40% (which covers relevant deviations) and the input uncertainty was increased to 20% for low frequencies (which is a rough empirical value), in order to take also modeling errors into account. For this case, the controller gain had to be set to $R = -3000$ to preserve robust stability. But also for this gain, the vibration control works still quite well on the nominal system, as it can be seen in Fig. 8.

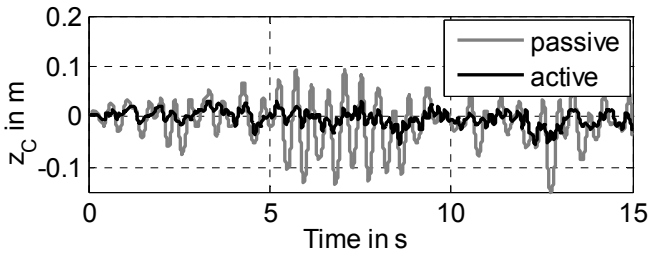

Fig. 8. Simulation of $z_C(t)$: passive vs. active system

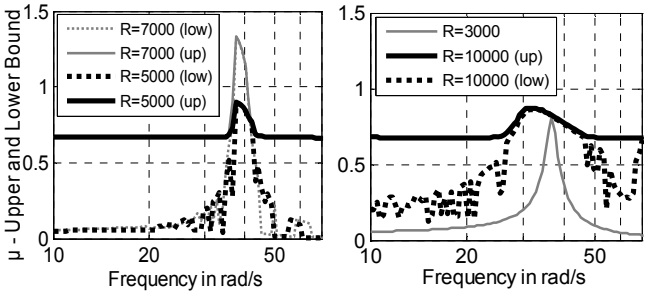

Fig. 9. μ-bounds for $\dot{z}_C$-feedback for different controllers

8. CONCLUSIONS

For an active suspension test-rig a nonlinear model was derived and linearized in the equilibrium point. Using the concept of trim point uncertainties, the theoretical basics for some innovative robust μ synthesis and analysis methods could be outlined which take the variation of the chassis mass into account. The idea was illustrated with a robust stability analysis example. Future work will treat the exact identification of all system components and the comparison of different controllers with the proposed methods. Finally the developed control designs must be validated by testing them on the test-rig or even a real quadricycle. Furthermore the approaches can be improved by using e.g. skew-μ synthesis or gain-scheduled and nonlinear controllers.

REFERENCES

Balas, G., Doyle, J., Glover, K., Packard, A., Smith, R. (1998). *μ-Analysis and Synthesis Toolbox User's Guide,* Musyn Inc. and The MathWorks, Inc.

Canudas de Wit, C., Aström, K.J., Lischinsky, P. (1995). A New Model for Control of Systems with Friction. *IEEE Transactions on Automatic Control,* **Vol. 40, NO. 3,** pp. 419-425.

Fialho, I., Balas, G.J. (2000). Design of Nonlinear Controllers for Active Vehicle Suspensions using Parameter-Varying Control Synthesis. *Journal of Vehicle Systems Dynamics,* **Vol. 33,** pp. 351-370.

Goldstein, H., Poole, C.P., Safko, J.L. (2002). *Classical Mechanics*, Third edition, Addison Wesley, ISBN: 0201657023.

Hecker, S. (2007). Generation of low order LFT Representations for Robust Control Applications Fortschrittberichte *VDI*, **Series 8, NO. 1114**, VDI-Verlag , Düsseldorf.

Herrnberger, M., Heller, P., Paul, R., Hecker, S., Sachs, G. (2007): Advanced Uncertainty Modeling and Robustness Analysis for the Basic Flight Control System of a Modern Jet Trainer. *AIAA Guidance, Navigation, and Control Conference and Exhibit*, AIAA-2007-6668.

Lauwerys, C., Swevers, J, Sas, P. (2004). Design and experimental validation of a linear robust controller for an active suspension of a quarter car. *Proceeding of the 2004 American Control Conference,* pp. 1481-1486.

Mäder, D. (2007). *Detailed Nonlinear Modeling of the Suspension of a Quarter Car Test-Rig and Analysis of Modern Control Approaches*, Student project, Institute of Automatic Control, Technische Universität München.

Mitschke, M., Wallentowitz, H. (2004). *Dynamik der Kraftfahrzeuge*, Springer, Berlin.

Skogestad, S., Postlethwaite, I. (1996). *Multivariable Feedback Control*, John Wiley & Sons. Chichester.

Venhovens, P.J.T. (1993). *Optimal Control of Vehicle Suspensions*, PhD thesis, Delft University of Technology, ISBN 90-370-0093-2.

Zhou, K., Doyle, J., Glover, K. (1996). *Robust and Optimal Control*, Prentice Hall, Inc., New Jersey.